Riverbed Clogging Associated with a California Riverbank Filtration System: An Assessment of Mechanisms and Monitoring Approaches

Craig Ulrich[a], Susan S.Hubbard[a], Joan Florsheim[b], Donald Rosenberry[c], Sharon Borglin[a], Marcus Trotta[d], Donald Seymour[d]

[a] Lawrence Berkeley National Laboratory, United States
[b] University of California – Santa Barbara, United States
[c] U.S. Geological Survey, United States
[d] Sonoma County Water Agency, United States

Available online 13 August 2015.

https://doi.org/10.1016/j.jhydrol.2015.08.012Get rights and content

Highlights

- Approach developed to identify abiotic and biotic influences to riverbed clogging.
- Riverbed clogging dominated by biological processes at a riverbank filtration site.
- Riverbed clogging influenced by seasonal effects and downstream dam operations.
- Benefits/limitations of seepage and thermal measurements, ERT, and cryocores.

Summary

An experimental field study was performed to investigate riverbed clogging processes and associated monitoring approaches near a dam-controlled riverbank filtration facility in Northern California. Motivated by previous studies at the site that indicated riverbed clogging plays an important role in the performance of the riverbank filtration system, we investigated the spatiotemporal variability and nature of the clogging. In particular, we investigated whether the clogging was due to abiotic or biotic mechanisms. A secondary aspect of the study was the testing of different methods to monitor riverbed clogging and related processes, such as seepage. Monitoring was conducted using both point-based approaches and spatially extensive geophysical approaches, including: grain-size analysis, temperature sensing, electrical resistivity tomography, seepage meters, microbial analysis, and cryocoring, along two transects. The point monitoring measurements suggested a substantial increase in riverbed biomass (2 orders of magnitude) after the dam was raised compared to the small increase (∼2%) in fine-grained sediment. These changes were concomitant with decreased seepage. The decreased seepage eventually led to the development of an unsaturated zone beneath the riverbed, which further decreased infiltration capacity. Comparison of our time-lapse grain-size and biomass datasets suggested that biotic processes played a greater role in clogging than did abiotic processes. Cryocoring and autonomous temperature loggers were most useful for locally monitoring clogging agents, while electrical resistivity data were useful for interpreting the spatial extent of a pumping-induced unsaturated zone that developed beneath the riverbed after riverbed clogging was initiated. The improved understanding of spatiotemporally variable riverbed clogging and monitoring approaches is expected to be useful for optimizing the riverbank filtration system operations.

1. Introduction and background

Riverbank Filtration (RBF) systems consist of high capacity pumping wells that are located adjacent to or beneath rivers. RBFs produce water by taking advantage of the natural processes that occur as surface water migrates through the riverbed (Jaramillo, 2012, Stuyfzand et al., 2006), such as adsorption, reduction, physicochemical filtration, sediment filtration, and biodegradation (Tufenkji et al., 2002). Riverbed clogging reduces hydraulic conductivity of the riverbed materials and thus limits infiltration of surface waters toward the collection wells. The clogging can impose a serious limitation to the rate and volume of water production associated with RBFs (Jaramillo, 2012, Schubert, 2006a, Schubert, 2006b, Sophocleous, 2002, Stuyfzand et al., 2006, Treese et al., 2009).

Laboratory and field studies conducted over the last decade have linked clogging to a combination of mechanisms, including sedimentation of fine-grained particles (Cunningham et al., 1987, Hubbs, 2006, Ray and Prommer, 2006, Wett, 2006), and biological processes, including growth of microbes and algae as well as production of biogas (Battin and Sengschmitt, 1999, Engesgaard et al., 2006, Darnault et al., 2003, Nogaro et al., 2010, Seifert and Engesgaard, 2007). Although commonly recognized in practice, development of methods to monitor and distinguish between different types of clogging mechanisms remains a topic of research.

This study has two primary objectives. The first objective is to investigate clogging mechanisms, their spatiotemporal evolution, and key controls at a RBF system in California. The second objective is to document the benefits and limitations of various methods for monitoring riverbed clogging and hydrological properties with an objective to identify which combination of methods is optimal. We consider a variety of both conventional and novel characterization and monitoring methods, including: grain-size analysis, temperature sensing, electrical resistivity tomography, seepage meters, microbial analysis, and cryocoring. To our knowledge, this is the first study to investigate the spatiotemporal clogging mechanisms at a RBF facility and to determine an efficient suite of methods to monitor clogging and associated riverbed hydrodynamics. After a brief description of the study site and related research (Section 2), we describe the monitoring methodologies (Section 3) and then present the results of the data analysis (Section 4). Section 5 presents a discussion of the methods and an interpretation of the clogging mechanisms at the study site.

1.1. Riverbed clogging mechanisms and hydrological responses

Riverbed clogging associated with sediment deposition has been investigated under both laboratory and field conditions for decades. Cunningham et al. (1987) conducted a flume study using sediments having grain-sizes (silt and clay) less than 0.063-mm diameter to investigate infiltration characteristics as a function of flow velocity. They observed deposition of fine-grained sediment at low flume flow velocities [<18 cm/s]; above a flume velocity of 18 cm/s they observed a steady degradation of the surficial fine-grained clogging layer. Schälchli (1992) conducted flume studies using riverbed sediments and found that hydraulic conductivity decreased by a factor of 9 within 100 h due to intrusion of fine sediments into the open pore space. Using seepage meters, and sediment cores, Nowinski et al. (2011) monitored the evolution of hydraulic conductivity

on a riverbed point bar using slug tests and grain-size analysis. They observed a hydraulic conductivity decrease by a factor of 4; this decrease was associated with a 10% increase in fine-grained sediments.

Clogging of riverbeds can also be caused by biological mechanisms, including the colonization of algae, diatoms, bacteria, extracellular polymeric substance (EPS), and subsequent biofilm build-up at the sediment–water interface and in the sediment pore spaces. Many different parameters affect biofilm development, including concentrations of organic matter and oxygen, nutrient flux, temperature, bacterial abundance and type, water depth, stream velocity, and pumping rate (Baveye et al., 1998, Engesgaard et al., 2006, Flemming et al., 2007, Jaramillo, 2012, Nogaro et al., 2010, Schijven et al., 2003, Seifert and Engesgaard, 2007). Both Engesgaard et al., 2006, Vandevivere and Baveye, 1992investigated biotic clogging in column experiments, and reported that bioclogging decreased relative bulk hydraulic conductivity by a factor of 100 within 30 days. Naranjo et al. (2012) reported a reduction in both hydraulic and thermal properties as a result of streambed clogging (internal colmation) in the down welling areas of a riffle-pool sequence. Flemming et al. (2007), who also investigated biotic clogging in column experiments, reported a decrease in hydraulic conductivity by a factor of 7.5 after 15 days.

Under natural systems, biofilms can develop into mats or flocs (Seifert and Engesgaard, 2007). Battin and Sengschmitt (1999)investigated the spatiotemporal variation of bioclogging on the Danube River and documented a decrease in leakage coefficient (ratio between the hydraulic conductivity and sediment layer thickness) of a factor of ∼3.8 within the top 20 cm of the riverbed. They attributed clogging in this study to be due to the accumulation of dead bacterial assemblages associated with algae. Hoffmann and Gunkel (2011) investigated the effect of bioclogging and particle retention at the surface of a lakebed bank filtration site in Germany. They found up to 48% of the pore space in the upper 10 cm of riverbed sediments was occupied by particulate organic matter (diatoms, biofilms, benthic algae, and detritus), which led to a hydraulic conductivity decrease by a factor of 100 in late autumn. Thullner et al. (2002) numerically modeled homogeneous versus heterogeneous pore size distributions with biomass growth (colony vs. biofilm) in sediments of various grain-sizes and sorting. Their simulations suggested that poorly sorted sediments experienced the greatest clogging, revealing a hydraulic conductivity decrease up to a factor of 100. Using a sand–gravel sediment in laboratory flume studies, Salant (2011) found that both bacteria and algae biomass are equally capable of surficial clogging.

Clogging at RBF facilities can be further exacerbated by the development of a pumping-induced unsaturated zone beneath the riverbed or lake bed. This occurs when the pumping rate exceeds the infiltration rate, at which time the piezometric (groundwater) head drops below the riverbed elevation and air is drawn below the bed from the shore margin (Hubbs, 2006, Zhang et al., 2011). Creation of an unsaturated zone beneath the riverbed can entrap air in the pore space, resulting in decreased hydraulic conductivity, infiltration and water production (Hubbs, 2006, Su et al., 2007, Zhang et al., 2011). Hubbs (2006) indicated that unsaturated zones beneath a river have a reduced ability to support the overburdened weight of the river, which can also result in sediment compression and permeability reduction.

1.2. Methods for monitoring riverbed clogging and hydrological responses

Many methods have been used to investigate riverbed clogging mechanisms and associated hydrological responses. In this section, we provide a short summary of traditional as well as less conventional approaches, many of which are used in our study.

Seepage meters have been used for over four decades to estimate riverbed infiltration. Seepage meters, which often consist of an open 55 gallon drum, utilize the natural movement of water to estimate seepage through riverbeds (Lee and Cherry, 1979). The basic mechanics of a seepage meter entail inserting the open end of a seepage meter ~10 cm into the riverbed. A bag filled with a known volume of water is attached by a hose to the seepage meter. Water flux across the sediment–water interface alters the volume of water in the bag (Lee and Cherry, 1979); calculation of the change of volume over time yields seepage rate and direction. Rosenberry and Pitlick, 2009, Rosenberry et al., 2012 and others have successfully used seepage meters to quantify spatiotemporal variations of hyporheic exchange in riverbeds.

Heat as a tracer (temperature flux) methods are commonly used to monitor seepage and hyporheic exchanges. In riverine systems, surface water is heated by daily cyclical radiant heating and cooling (Blasch et al., 2007). The propagation of temperature from river water into the subsurface is assumed to be governed by conduction, advection, and/or dispersion (Battin and Sengschmitt, 1999, Constantz, 2008). As the oscillating temperature signals propagate, the temperature signal is attenuated from interaction with sediments and, where present, upwelling and/or downwelling water (Battin and Sengschmitt, 1999). The degree to which thermal gradients propagate in the subsurface also depends on the thermal properties of water and sediments (Hatch et al., 2006). Highly sampled logs of daily temperature variations at different riverbed depths are used to measure temporal changes. Shifts in the temperature amplitude and peak-lag (phase) between vertical temperature sensors have been used to estimate hydraulic properties (Constantz et al., 2004, Cox et al., 2007, Gordon et al., 2012, Hatch, 2007, Hatch et al., 2006, Lautz, 2012). When combined with vertical hydraulic-gradient measurements from piezometers installed beneath the riverbed (Gorman, 2004, Lee and Cherry, 1979) hydraulic conductivity can also be estimated (Constantz et al., 2004, Su et al., 2003, Su et al., 2004). If hydraulic gradients are not available, time series distribution of the thermal records can also be used to estimate seepage (Hatch, 2007, Hatch et al., 2006, Shanafield et al., 2011).

Mechanical coring devices (shovel, augers, probes, etc.) are often used to collect riverbed sediments, which in turn are used to determine grain-size distribution using laboratory techniques. Hydrological properties can be measured using laboratory head tests or estimated using grain-size information (Bunte and Abt, 2001, Cunningham et al., 1987, Gorman, 2004, Hubbs, 2004, Hubbs, 2006, Kondolf et al., 2005). Many relationships have been developed to relate grain-size distributions to hydraulic conductivity, including Hazen, 1892, Kozeny, 1927 and others as reviewed by Chapuis, 2012, Odong, 2007. Grain-size analysis from cores collected in riverbeds over time has been used to assess changes in riverbed permeability (Gorman, 2004, Lisle, 1989, Nowinski et al., 2011, Zimmermann et al., 2005). Several of these studies highlight the difficulty of collecting representative sediment cores using conventional methods due to loss of fines during sample collection and the challenges of working in standing or moving water.

Cryocoring (or freeze coring) is a device that enables riverbed sampling of 'intact' sediments, pore fluids, and biotic material. Cryocoring involves using liquid nitrogen to freeze intact sediments and pore fluids by flowing the liquid nitrogen inside of pipes inserted into the sediments of interest and then extracting the pipe with attached frozen sediments. If performed over time within a small region, cryocoring can be used to monitor the evolution of riverbed microbiological agents (microbes, biofilms, algae) that lead to bioclogging (Blaschke et al., 2003, Hoffmann and Gunkel, 2011); as well as changes in grain-size distributions (Bianchin et al., 2011, Blaschke et al., 2003, Hanrahan et al., 2005, Moser et al., 2003, Schälchli, 1992).

Electrical resistivity tomography (ERT) has recently been explored as a method to monitor surface water–groundwater exchanges (Cardenas and Markowski, 2010, Crook et al., 2008, Mitchell et al., 2008, Nyquist et al., 2008, Nyquist et al., 2010, Schwartz et al., 2008, Singha and Gorelick, 2006, Slater et al., 2010, Ward et al., 2010). Resistivity is a measure of the ability of a material to resist electrical current flow; it is the inverse of electrical conductivity and is an intrinsic property of the sediment. In electrical resistivity methods, a typically low frequency (<1 Hz) current is injected into the ground between two current electrodes, while one or more pairs of potential electrodes are used to measure electrical potential differences. At the low frequencies measured and in this coarse-grained riverbed system, energy loss is dominated by ionic conduction. Ionic conduction results from the electrolyte filling the interconnected pore space (Archie, 1942) as well as from surface conduction via the formation of an electrical double layer at the grain-fluid interface (e.g., Revil and Glover, 1997, Revil and Glover, 1998). Because electrical resistivity is sensitive to moisture content, salinity, temperature and clay content (e.g., Lesmes and Friedman, 2005), it can be useful for characterizing and monitoring river systems.

Most resistivity surveys utilize a four-electrode measurement approach. To obtain a value for subsurface resistivity, two potential electrodes are placed at some distance from the current electrodes, and the difference in electrical potential or voltage is measured. This measurement, together with the injected current and the geometric factor, which is a function of the particular electrode configuration and spacing, can be used to calculate resistivity values for subsurface conditions following Ohm's law. In river systems, ERT can be collected by installing electrodes in the riverbed, by towing cables along the surface of the water body, or by resting cables on the riverbed. Common multi-channel ERT acquisition systems can permit tens to hundreds of electrodes to be used alternatively as both current and potential electrodes to obtain two- or three-dimensional electrical resistivity models (e.g., Günther et al., 2006). Inversion of these data is performed to estimate the spatial distribution of electrical resistivity (e.g., Binley and Kemna, 2005, Constable et al., 1987, deGroot-Hedlin and Constable, 1990).

ERT has been successfully used to investigate geologic features controlling seepage into lakes and rivers (Mitchell et al., 2008, Nyquist et al., 2008, Nyquist et al., 2009), contaminant seepage to a river (Slater et al., 2010), hyporheic exchange and flow paths when paired with a saline tracer test (Nyquist et al., 2010, Toran et al., 2013, Ward et al., 2012, Ward et al., 2010), natural groundwater and stream water mixing in the hyporheic

zone in time-lapse (Cardenas and Markowski, 2010), and riverbed saturation (Miller et al., 2008). To our knowledge, ERT has not been used to investigate hydrodynamics associated with RBF-related clogging.

2. Wohler RBF study site and related research

2.1. Wohler RBF study site

The Russian River is a perennial river that has headwaters in Mendocino and Sonoma County, California and meanders south by southwest, where it finally discharges into the Pacific Ocean at Jenner, California. The region has a Mediterranean climate and an annual rainfall of 1.04 m (Gorman, 2004) that occurs between November and May with virtually no rain throughout the summer months when water demand is greatest. The Sonoma County Water Agency (SCWA) operates an RBF system that supplies water to over 600,000 people and is a vital artery of water supply for the county. We investigated a reach of the Russian River, located approximately 37 km upstream from the mouth of the river that is adjacent to the SCWA RBF Facility near Forestville, California (Fig. 1). SCWA's RBF is comprised of six radial collector wells that have a total production capacity estimated to be approximately 92 million gallons/day (MGD); however, substantial variations to this estimated capacity can occur due to seasonal variations in river flows, operation of infiltration ponds, and sedimentation patterns along the riverbed. SCWA's RBF system also includes seven vertical wells to be used as reserve capacity wells. The SCWA seasonally operates a downstream (1.2 km) inflatable dam that creates backwater conditions and increases the stage of the river and hydraulic heads in the adjacent aquifer, resulting in increased infiltration in the Wohler area and enhanced production capacity of Wohler Collector wells 1, 2, and 6. Inflation of the dam also allows for operation of five infiltration ponds located downstream of the study site to recharge the aquifer in the vicinity of Mirabel Collector wells 3, 4, and 5. Generally, the operations of the facility are governed by demand and season (rainy or dry); the dam is usually inflated from May to November (dry season) to improve water production (river flow ~90 to 125 cfs) and is lowered from November to May due to high storm-flow events (up to 30 k cfs) (from personal communication with SCWA).

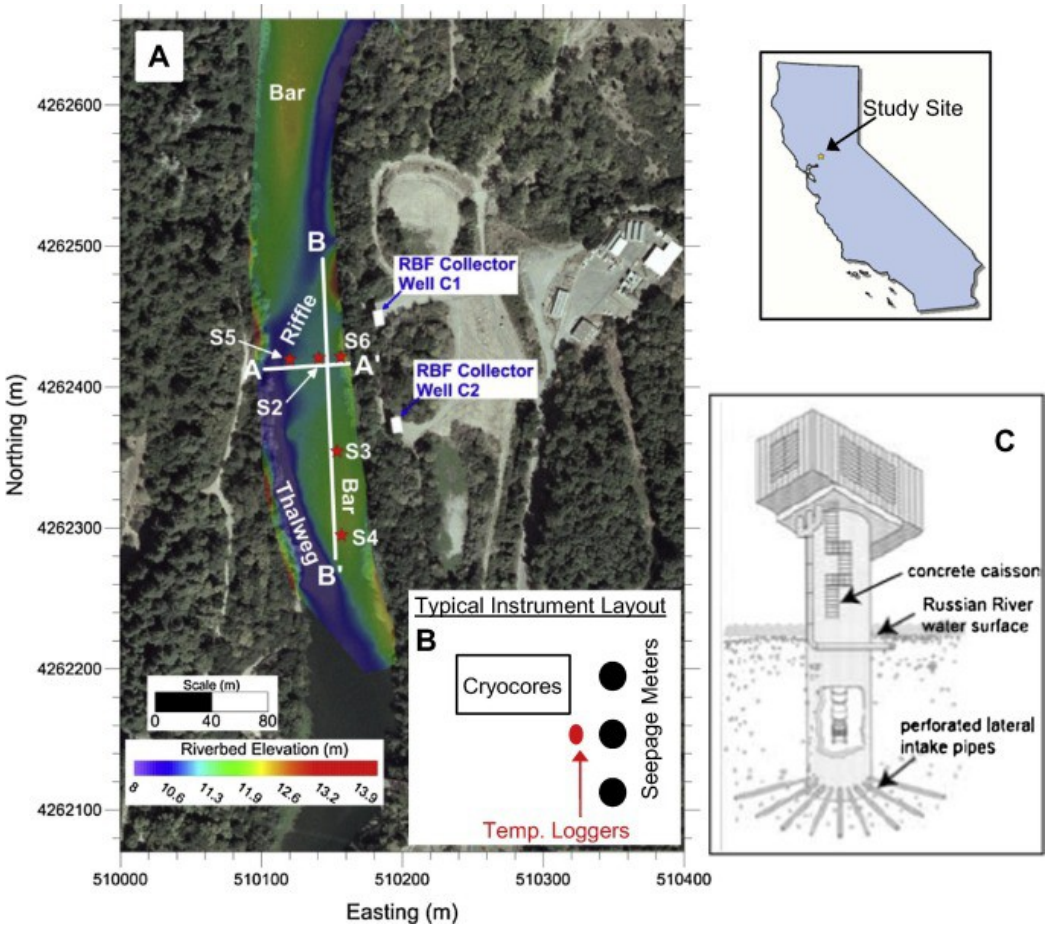

Download high-res image (805KB)
Download full-size image

Fig. 1. The Wohler field study site, located on the Russian River near Forestville, CA. Riverbed elevations indicated were measured in May of 2012. (A) Measurement locations S2, S3, S4, S5, S6 (seepage meters, cryocores, and temperature loggers at each location) and ERT profiles (white lines). (B) Typical instrumentation layout for each of the five measurement locations. (C) RBF collector well schematic (laterals extend from the bottom of the well approximately 20 m below the ground surface).

The study area encompasses a 200-m long by 70-m wide portion of the Russian River located adjacent to SWCA's RBF Collector wells 1 and 2 (Fig. 1). This particular reach of the Russian River is located within a natural bedrock constriction where the river valley narrows from an average of 1.6–3.2 km wide upstream of the study site to 0.1 miles wide at the study site, which causes a natural backwater effect upstream of the study site. The Russian River at the study site is underlain by unconsolidated alluvial sands and gravels with sporadic intermittent silt/clay lenses. These alluvial sediments are poorly sorted and generally range between 15 and 30-m thick (Gorman, 2004). The alluvial sediments are underlain by fractured shale bedrock of the Franciscan Complex (Gorman, 2004). Collector wells 1 and 2 are about 80 m apart. Each well includes 9–12 horizontal laterals that extend from the bottom of the well (approximately 20 m below the ground surface) in a radial direction toward and in some cases beneath, the river (Fig. 1C).

2.2. Previous related research at Wohler

Several experimental and numerical studies have been performed at the Wohler RBF. Tracers such as heat, chloride, and specific conductance have been used to estimate riverbed seepage rates (Constantz et al.,

2004, Cox et al., 2007, Hatch, 2007, Su et al., 2003, Su et al., 2004). Constantz et al. (2004) used temperature profiles and hydraulic gradient measurements to estimate seepage and hydraulic conductivity ($K = 4.1 \times 10^{-3}$ cm/s) and observed that seepage varies spatially and temporally. Gorman (2004) used seepage meters, piezometers, and grain-size analysis from samples recovered using shovels to evaluate changes in hydraulic conductivity in relation to riverbed clogging. Gorman (2004) found that seepage rates varied spatially across the river; the rates were highest near the thalweg (channel) and lowest in the center of the river at the toe of a bar (approximately 20–30 m away from the thalweg). Gorman (2004) attempted to quantify the grain-size characteristics of the riverbed throughout the season, but unfortunately the majority of the surface fines were lost due to winnowing during sample retrieval. Using thermal profiles, Constantz et al. (2004) also documented the lowest seepage rates in the center of the river and interpreted them to be due to the presence of a subsurface low permeability layer.

Several numerical studies have also been performed to quantify hydrological behavior associated with the Wohler RBF. Su et al. (2004) used the thermal and hydraulic measurements to parameterize a numerical model. They found that the initial hydraulic conductivity of the streambed led to good correspondence between predicted and observed thermal profiles from May to August but they had to decrease hydraulic conductivity by 60% to fit modeled August temperatures near the production wells. They attributed this decrease in hydraulic conductivity to deposition of fine sediment and organic material on the riverbed surface. Su et al. (2007) performed a series of simulations of the system using different constant values for riverbed permeability (2.4×10^{-10}–7.4×10^{-13} m^2). Regardless of riverbed permeability value, their simulations suggested that pumping led to the development of an unsaturated zone located approximately 2-m below the riverbed that extended ~25-m in width and ~130-m along the river axis. Zhang et al. (2011) refined this model by incorporating a dynamic riverbed permeability function and additional constraints, including pumping rate, river stage, and groundwater temperature from monitoring wells (3–7 m below the riverbed) located adjacent to the river. Their simulations suggested that permeability decreased throughout the dry season, leading to a permeability reduction by a factor of 2.5. They performed a sensitivity analysis that indicated infiltration was most sensitive to riverbed permeability followed by pumping rate and river stage. Although Zhang et al. (2011) documented the importance of (and estimated) a dynamic riverbed permeability function; the function was based on numerical inversion rather than on an understanding of the key controls on dynamic riverbed permeability. The motivation for the study described in this manuscript was to develop a better understanding of these controls and their spatiotemporal variability in order to further improve predictive modeling of RBF behavior at Wohler.

3. Acquisition campaigns and monitoring datasets

A variety of techniques were used to explore clogging mechanisms at the Wohler RBF (Fig. 1 and Table 1). The study area includes five measurement stations (S2–S6, Fig. 1A) located along two transects. The river geomorphology in the study area is composed of a thalweg (river channel), bars, and riffle (high river velocity zone between deeper thalweg regions) (contours Fig. 1A). Measurement station S5 is geomorphically unique in that it is situated on the shoulder of the thalweg. Measurement station S2 is in a riffle, S3 and S4 are on a gravel bar, and S6 is at the near bank; stations S2–S6 are all topographically similar. The RBF laterals extend to

the east bank of the river near S6. Stations S2, S3, and S4 are aligned along the longitudinal river axis, while S2, S5 and S6 traverse this axis.

Table 1. Timeline and description of data acquisition methods and field observations. Fig. 2 shows graphically river stage versus campaign.

Date	Data collected	RBF operations	Field observations
May 28th–June 6th Campaign 1 '*Initial riverbed inundation period*'	ERT, cryocores, seepage meters installed: temperature loggers	Raised dam May 28th, collectors pumping at ~10 to 20 mg/d	Riverbed scoured by previous winter flows, no fines or microbial growth observed
July 30th–31st Campaign 2 '*Inundated*'	ERT	Pumping	Riverbed is covered by algal bloom and river water is murky and greenish with fines developing on surface
September 10th–14th Campaign 3 '*Inundated*'	ERT, sryocores, seepage meters	Pumping	River temperature is colder, algal bloom has partially died, ~1 cm thick brown mat covering most of riverbed but dislodges easily and floats away leaving riverbed somewhat clean
November 7th–16th Campaign 4 '*Inundated*'	ERT, cryocores, Seepage meters, and temperature loggers	Dam lowered the following week	River temperature is colder still, all algal are dead, ~2 cm thick brown mat covering riverbed, but dislodges easily and floats away leaving riverbed somewhat clean

Many measurements were collected at each station (Fig. 1B) including cryocores, temperature loggers, and seepage meters. Measurements could not be made in the center of the thalweg due to the depth and higher flow velocity. Data were collected during 4 campaigns (Fig. 2) as follows: Campaign 1 was performed directly after the inflatable dam was raised; we consider this initial inundation period as the background campaign. Campaigns 2, 3, and 4 were conducted after the river was fully inundated. Table 1describes the data acquisition campaigns, methods, and RBF operations.

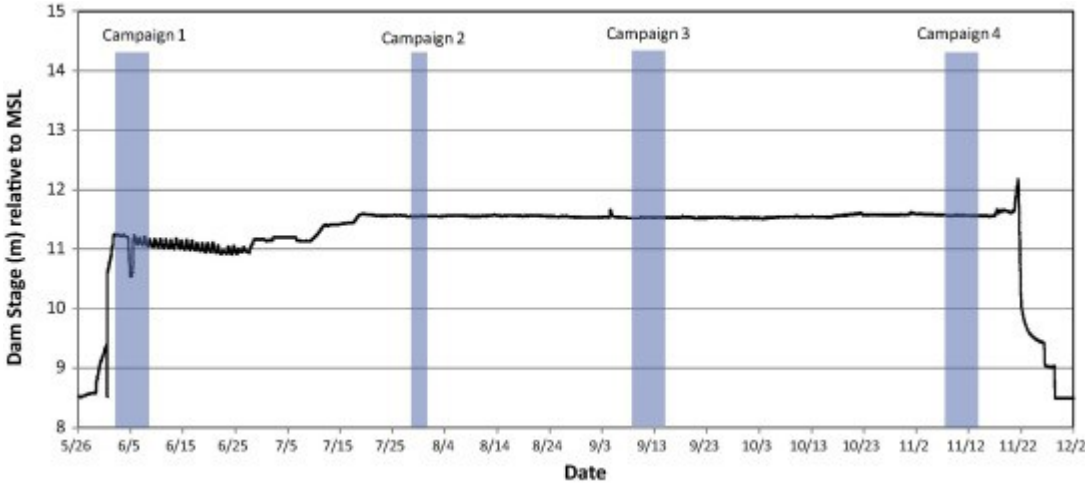

Download high-res image (149KB)

Download full-size image

Fig. 2. River stage and associated data collection campaigns. Campaign duration is indicated by the blue hachured zones.

3.1. Heat as a tracer

Vertical temperature profiles were installed at each of the five measurement stations to investigate the change in riverbed seepage from May to November 2012. Three stand-alone Onset Hobo Pendant temperature loggers were installed inside a steel pipe and driven 1 m into the riverbed at 20 cm, 50 cm, and 80 cm below the riverbed at each of the five locations. The total depth of the installed pipe was limited by the ability to physically install 2″ diameter pipe in the riverbed. The temperature sensors were set to record data every 10 min. One reference data logger was also placed approximately 1-cm off the riverbed in the surface water in the center of the survey area to log the daily diurnal temperature variation. Onset specifications state the measurement range of these particular data loggers as −20 to 70 °C with an accuracy of ±0.53 °C and a resolution of ±0.25 °C. Seepage estimates were derived from thermal gradients using the time series analysis method developed by Hatch et al. (2006). To expedite the conversion of temperature gradient to seepage flux values, we used the Vertical Fluid Heat Transfer Solver (VFLUX) program. This program calculates one-dimensional vertical fluid flow through saturated media using heat transport equations from the Hatch method (Gordon et al., 2012), which filters each time series using a Dynamic Harmonic Regression (Captain Toolbox, [Young et al., 2010]) to isolate the fundamental frequency of the thermal signature and extract the amplitude and phase of the signal. The amplitude and phase shifts between two sensors (along with estimates of the sediment and fluid thermal properties) are used to estimate flux between the referenced sensors. The approach was used with the Wohler data to estimate seepage flux from sixteen temperature sensors and roughly 400,000 data points.

3.2. Seepage meters

Fifteen seepage meters were installed during three sampling campaigns with three seepage meters at each location (Fig. 1B). The seepage meters were installed at the beginning of each of the three campaigns so the portion of the riverbed covered by the meters would not be disturbed from other data collection activities. Three data collection rounds were made at each seepage meter to calculate the average seepage rate at each of the five locations. Seepage meters were constructed using the bottom and top thirds of a 55-gallon steel drum inserted 10 cm into the riverbed and fitted with a seepage bag that was connected via a 16-mm-diameter garden hose (Lee and Cherry, 1979, Rosenberry, 2005, Rosenberry, 2008). Seepage bags (∼3 l) were housed in plastic shelters to protect the bag from measurement bias caused by the flowing river (Rosenberry, 2008). Each bag was filled with ∼2 l of river water and the measurement duration was based on a trial and error assessment because seepage rates varied greatly, requiring measurement periods that ranged from 3 min to 1 h to prevent emptying of the bag.

3.3. Grain-size analysis and microbial characterization using cryocoring approach

To investigate the seasonal accumulation of fine-grained sediment and microbial biomass at the riverbed interface, sediment cores were collected using the cryocore method based on a system described in Cahoon et al. (1996). Copper pipes were inserted into the riverbed and liquid nitrogen flowed downward into the pipe

freezing the sediment around the pipe (Cahoon et al., 1996). The cryocore was extracted from a depth up to 30 cm in the riverbed and promptly put into a cooler filled with dry ice to prevent core thawing, and transported back to the laboratory and placed into a −80 °C freezer for preservation. In order to maximize comparison of grain-size temporal variability using cores that were collected at different locations, each redundant core was collected within 15 cm of the 'background' May core location (within a 30 cm by 30 cm sampling plot), and all cores were collected within the same geomorphic feature. At the start of this study, four cores were collected on the same day at three locations (two cores at each location [S2, S3 and S4] and 1 m apart) to assess the sediment grain-size spatial variability at one point in time. For all campaigns post-baseline, two cryocores were collected at each sampling location, one for sediment grain-size analysis and one for microbial analysis. At the start of the campaign (May) water levels were low (initial inundation of the bars), which permitted the collection of cores at each of the five locations. However, water levels following full dam inflation at sites S2, S5, and S6 were roughly 2-m deep, which prevented the collection of cores during subsequent campaigns.

Cryocores collected for grain-size analysis were analyzed in accordance with ASTM C136-01 Standard Test Method for Sieve Analysis of Fine and Coarse Aggregates. The frozen cores were sectioned by depth (0–5 cm, 5–10 cm, 10–20 cm and 20+ cm) and dried at 110 °C in an oven until constant mass was observed (typically 24–36 h). After the dried mass was recorded the sample's organic content was investigated using the loss on ignition test (Dean, 1974, Heiri et al., 2001) and placed into the oven again at 500 °C and dried until constant mass to record the total organic content. The dried sample was then mechanically dry sieved by a RoTap machine and due to the wide range of particle sizes observed in the Russian River, a set of 21 sieves was used to complete the grain-size analysis; sieve openings ranged in diameter from 0.063 to 12 mm. Grain-size distribution curves were then generated for each sample as a whole core and for each of the sectioned depths following grain-size analysis. Statistical analysis showed the ranges of median and mean grain-size distributions at S2, S3 and S4 were very similar, with mean ranges of 4.5–5.2 mm, 4.8–5.0 mm and 4.9–5.3 mm, respectively. The percent sand fraction ranged between 34% and 38% for all six cores. The similarities in the spatial variabilities of the grain-size distributions within the 30 × 30 cm sampling area suggested that the baseline grain-size distributions can be considered as somewhat uniform within the area, As such, we make an assumption that time-lapse changes in grain-size associated with subsequent sampling at a single core location within the 30 × 30 cm intensive sampling area can be attributed to dynamic biotic or abiotic processes rather than to small lengthscale spatial variability.

Porosity (n) was empirically derived from the grain-size information following Vukovic and Soro's (1992) equation [$n = 0.255(1 + 0.83^{U})$ where U is the coefficient of grain uniformity [$U = (d_{60}/d_{10})$]. Odong (2007) compared multiple empirical formulas for determining hydraulic conductivity from grain-size of gravelly sands to fine sands. In all gravelly sands estimated in his study the Kozeny–Carmen formula most accurately estimated hydraulic conductivity compared to the Breyer and Hazen equations. For our study we decided to use the Kozeny–Carmen equation because the sediments in our study are gravelly sands. The Kozeny–Carmen relationship is given by

$$K = g/v * 8.3 \times 10^{-3} * (n^3/(1-n)^2) * d_{10}^2, \quad (1)$$

where g = acceleration of gravity; v = kinematic viscosity; n = porosity; and d_{10} = the sediment finer than ten percent. Odong (2007) determined that the Kozeny–Carmen relation performed best for sediments exhibiting uniformity coefficients (U) greater than 5. The U for sediments in our study area ranged from 9.5 to 17.

Colocated cryocores were also collected for microbial analysis and were sectioned at the same intervals and time as the grain-size analysis cores and analyzed by the Phospholipid Fatty Acid (PLFA) (Bouskill et al., 2012, Guckert et al., 1985, Pfiffner et al., 2006, White and Ringelberg, 1998) technique to determine the microbial communities and total biomass growing on the surface and at depth within the riverbed. The procedure to extract and analyze the biomass (the sum of all lipid species found) is described in the Supplementary Information. Lipid classes were grouped into biomass types according to chemical structure (Cusack et al., 2010, Griffiths et al., 1998, Moore-Kucera and Dick, 2008, Salomonová et al., 2003, Steger et al., 2003, White and Ringelberg, 1998). For example, all PLFA with one double bond in the chemical structure were assigned to the biomass group gram-negative bacteria.

3.4. Electrical resistivity tomography (ERT)

Two ERT profiles were collected in the study area, one (A–A′) that is perpendicular to the river axis and one (B–B′) that is located along the river axis (Fig. 1A). ERT profile A–A′ had the first 5 electrodes on land and the remaining 107 electrodes were submerged on the riverbed. Electrodes used for profile B–B′ were emplaced completely underwater. An eight-channel AGI SuperSting R8 Resistivity/IP meter was used with a 112-electrode (0.61 m *a*-spacing) marine multicore cable specially made for this survey with stainless steel electrodes and waterproof sheathing. A maximum current of 2000 milliamps (mA) was set during data acquisition but the system automatically steps down the current if less is needed; an average current of 320 mA was injected for 1.2 s for each measurement during this study. The resistivity survey used a dipole-dipole configuration and resulted in roughly 14715 data points. Contact resistances ranged from 933 to 1200 Ω. Data points with low voltage (<1 mV) and low current (<100 mA) accounted for less than 10% of the data and were removed prior to inversion. A full description of the ERT methodology, including model and inversion constraints (water depth and salinity, and water temperature [surface water and groundwater], and data error assessment) is described in the Supplemental Information. In brief, all data with low current (<100 mA) and low voltage (<2 mV) were removed prior to inversion, along with data with a repeat error over 3%. In total less than 8% of the data was removed prior to inversion. Effects from water salinity and temperature changes were analyzed from monitoring data. Salinity varied by a maximum of ∼5 Ω m between river water and groundwater throughout the season. Using a simple form of Archie's Law (full description in Supplemental Information) with a porosity of 0.27 from sediment analysis the range of expected bulk resistivity would be 200–231 Ω m when saturated with river water. Fluid temperatures varied by 5 °C throughout the season and by less than 0.5 °C during a single campaign. At 80 cm depth (deepest temperature sensors) daily temperatures varied by less than 0.5 °C and in a nearby monitoring well (30 m away and 15 m below ground surface) were 0.2 °C less than at 80 cm. Indicating little to no change between 80 cm and 15 m below the riverbed. ERT data were corrected for temperature effects from the riverbed surface to 1 m depth

following Keller and Frischknecht (1996). Given little to no change in salinity and temperature below 1 m changes in observed resistivity would result from changes in saturation.

4. Results

Results associated with Campaign 1 (initial riverbed inundation) will be presented for each method, followed by results for Campaigns 2–4 (post inundation) (refer to Fig. 2 and Table 1). A comparison of the results associated with different measurement approaches will be provided in Section 5.

4.1. Cryocore grain-size and biological results

Cryocore sampling was performed over time at all 5 measurement stations. Cumulative grain-size distribution summary results (d_{10}, d_{50}, and d_{60} in mm) of the recovered sediments from the May (Campaign 1) core analysis are shown in Table 2. In general, these data suggest that the sediments at the site during this time period are poorly sorted gravel and do not vary substantially with location or depth. At the riverbed surface and at depth, little fine-grained material (<0.074 mm) was observed (<1% mass retained). Total organic content, determined by Loss on Ignition (Dean, 1974) ranged from 0.5% to 4% mass dry weight.

Table 2. Sediment grainsize analysis summary. Distribution percentiles, d_{10}, d_{50}, and d_{60} in mm.

Core	Date	Depth (cm)	d_{10}	d_{60}	d_{50}
S2	May	24	0.5	5.6	4.5
S3	May	24	0.45	5.0	3.5
S4	May	24	0.32	5.2	3.8
S5	May	24	0.48	7.0	5
S6	May	24	0.3	5	3.1

Two cryocores at each location were collected at S2, S3, and S4 during September and at S3 and S4 during November; the depth of the river prohibited collection of cores at other locations and Campaigns. The grain-size distributions associated with the recovered sediments at S3 and S4 were similar to each other (Fig. 3A and B). This figure also shows the grain-size distribution as a function of season, revealing no consistent change in fine-grained sediments over time. Core S3 exhibited a 1.1% increase in fines (<1.0 mm) and core S4 exhibited a 1.2% decrease in fines between May and November. Deeper cores similarly did not display any constant grain-size trend over time (data not shown).

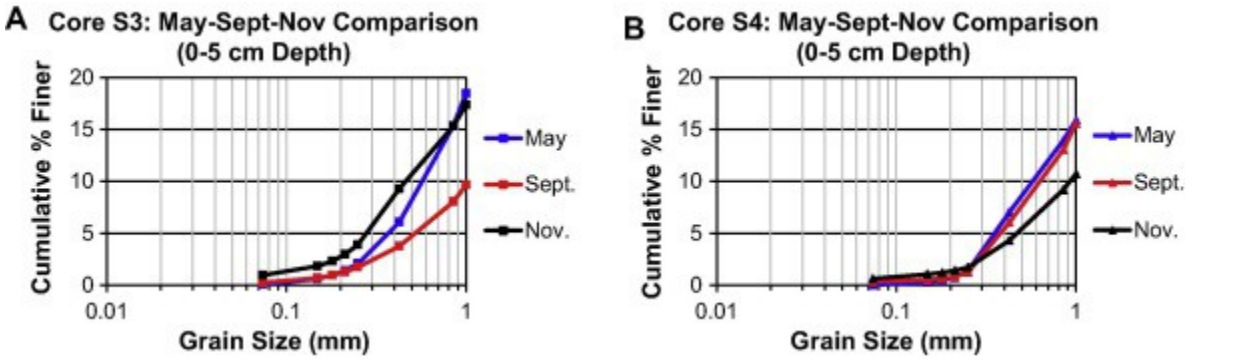

Download high-res image (239KB)

Download full-size image

Fig. 3. Grain-size distribution curves from cryocore-recovered samples showing the fraction of the samples that are finer than 1 mm portions for May, September, and November at locations (A) S3 and (B) S4. Different grain-size fractions either decrease or increase and no clear trend of increasing fines throughout the season is observed.

Hydraulic conductivity was estimated empirically using cores S3 and S4 (0–10 cm) grain-size distributions and the Kozeny–Carmen equation (Fig. 4). Porosity, calculated for each sample and at varying depths using d_{10} and d_{60} from the grain-size distribution curves, ranged from 0.27 to 0.29. The fluid viscosity parameter in the Kozeny–Carmen equation was corrected for temperature effects during each campaign. Fig. 4 shows estimated hydraulic conductivity from 0 to 10 cm for cores S3 and S4. Core S3 hydraulic conductivity decreased from May (65 m/day) to September (34 m/day) and increased again in November (37 m/day). Core S4 hydraulic conductivity increased from May to September and decreased from September to November. Overall throughout the season hydraulic conductivity decreased at station S3 and was relatively constant at station S4.

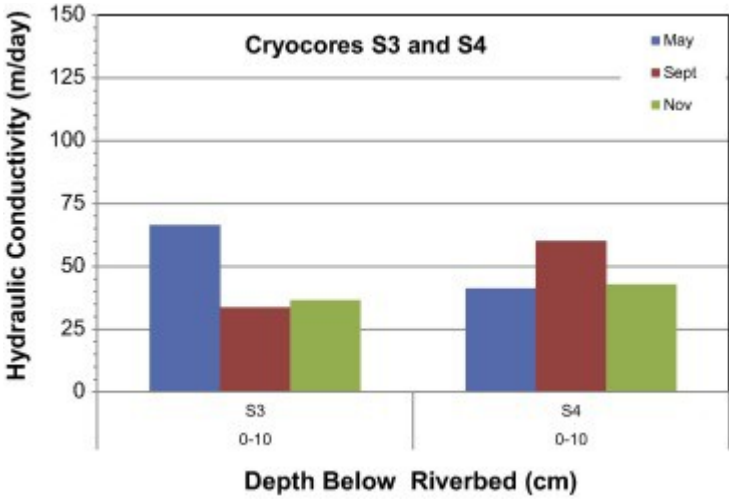

Download high-res image (105KB)
Download full-size image

Fig. 4. Hydraulic conductivity empirically estimated using the Kozeny–Carmen equation for cryocores S3 and S4. The estimates display both spatial and temporal variations in hydraulic conductivity by season.

Results from the May microbial PLFA analysis of all six cores show little to no biomass throughout all depths: Fig. 5 shows data associated with cores S3 and S4. The only anomaly is at S6 in the 0–10 cm (not shown) section where the biomass count is 6–23 times higher than the other samples at the same depth interval. We expect this anomaly is due to the sample location proximity to the east river bank, which was covered with living waterborne plants and a several cm thick layer of fine sediment. Fig. 5B suggests algae content is negligible during May and that the biomass is dominated by bacteria.

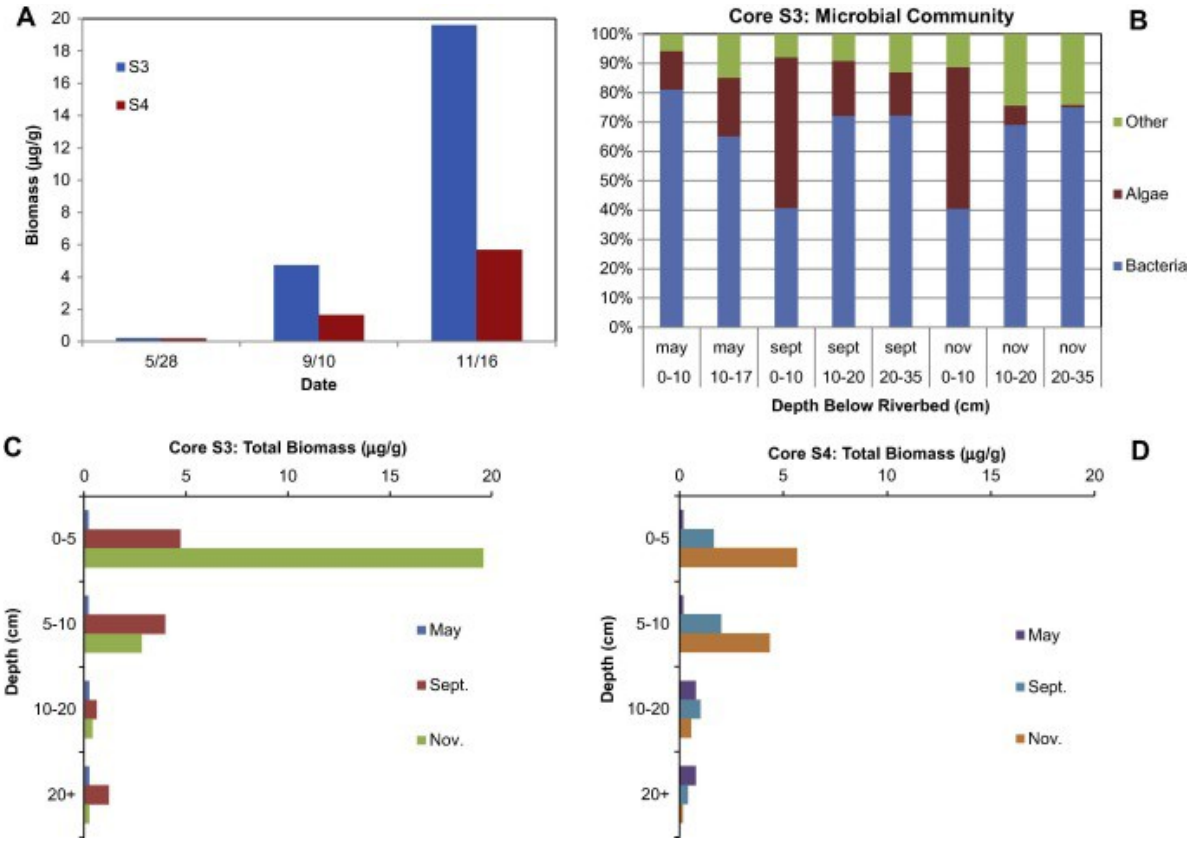

Download high-res image (335KB)
Download full-size image

Fig. 5. Microbial total biomass results from the PLFA analysis at core locations S3 and S4 during May, September, and November campaigns. (A) Low biomass was observed in May at both measured stations, followed by substantial increase in biomass observed during September and November (B) S3 microbial community, showing that the riverbed system was dominated by bacteria in May and that algae content increased substantially in September and November. (C and D) Biomass decreased with depth and also revealed seasonal trends at stations S3 and S4.

PLFA analysis of core S3 and S4 collected during subsequent campaigns show that biomass growth in 0–5-cm depth increased by more than an order of magnitude (0.2–4.7 µg/g, Fig. 5C) from May to September, and by almost two orders of magnitude (0.2–19.7 µg/g, Fig. 5C) from May to November. Core S4 was the only other location where three replicate samples were collected; each revealed a similar trend at the 0–5-cm depth (Fig. 5D). Total biomass for both S3 and S4 also increased throughout the season from 5 to 10 cm depth, and biomass decreased at depths below 10 cm to almost insignificant levels. During the September campaign, algae represented ~50% of the microbial community in the top 10 cm whereas bacteria represented ~75% of the community below 10 cm (Fig. 5B). Algae content was also significant during the November campaign, representing ~50% of the community in the top 10 cm. Bacteria again dominated the deeper (>10 cm) microbial community (Fig. 5B).

4.2. Seepage meter results

Fig. 6 shows that May average seepage rates (averaged from three seepage meters measured simultaneously and spaced one meter apart) were spatially and temporally variable and ranged from +2.0 (upward) to −216 cm/d (downward). Seepage at measurement station S5 (on the shoulder of the thalweg) was greatest

and accounts for 90% of the total seepage measured in May. Seepage results during September show decreased infiltration near the thalweg (S5 = −105 cm/d) and increased infiltration at all other locations (Fig. 6). Even with increased seepage at all other locations, S5 still accounts for 60% of the total September measured seepage. November average seepage rates ranged from −0.4 to −70.5 cm/d with the highest again at S5, accounting for more than 85% of the total November measured seepage.

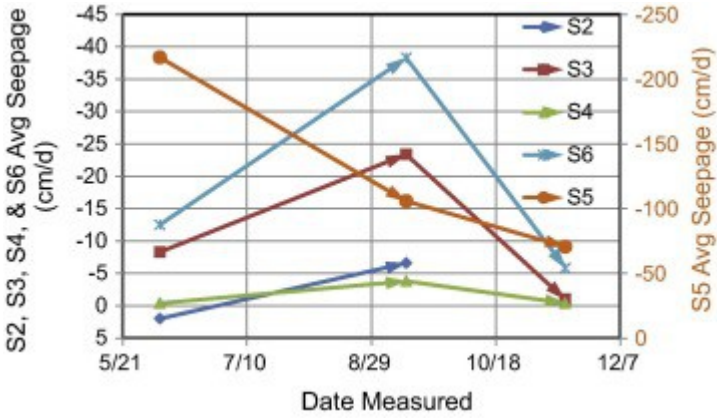

Download high-res image (181KB)
Download full-size image

Fig. 6. Average seepage for each location throughout the season (May–November). S5 (in orange) is located in the thalweg has much higher seepage compared to other locations. Stations S2, S3, and S4 are located in the middle of the river along the long axis and S6 is near the bank. (For interpretation of the references to color in this figure legend, the reader is referred to the web version of this article.)

4.3. Temperature based seepage estimates

The temperature data were used to estimate seepage using the VFLUX program: raw thermal logs (Fig. S1) and sensitivity analysis data (Table S1) are provided in the Supplementary Information. Thermal properties for the fluid and sediments were obtained from previous studies at this site by Hatch, 2007, Su et al., 2004. Fig. 7shows comparisons of seepage rates obtained from seepage meters and estimated from temperature sensors at S2, S3, and S5. The difference between the seepage estimates obtained using the two methods may be due to the uncertainty of sediment thermal property estimates (from Hatch, 2007, Su et al., 2004) used in the VFLUX program and/or to the representative volume associated with the different techniques. Given the consistent trends and the temporal density of the temperature data relative to the seepage meters, in the remainder of the study we rely on the temperature based estimates for our interpretation.

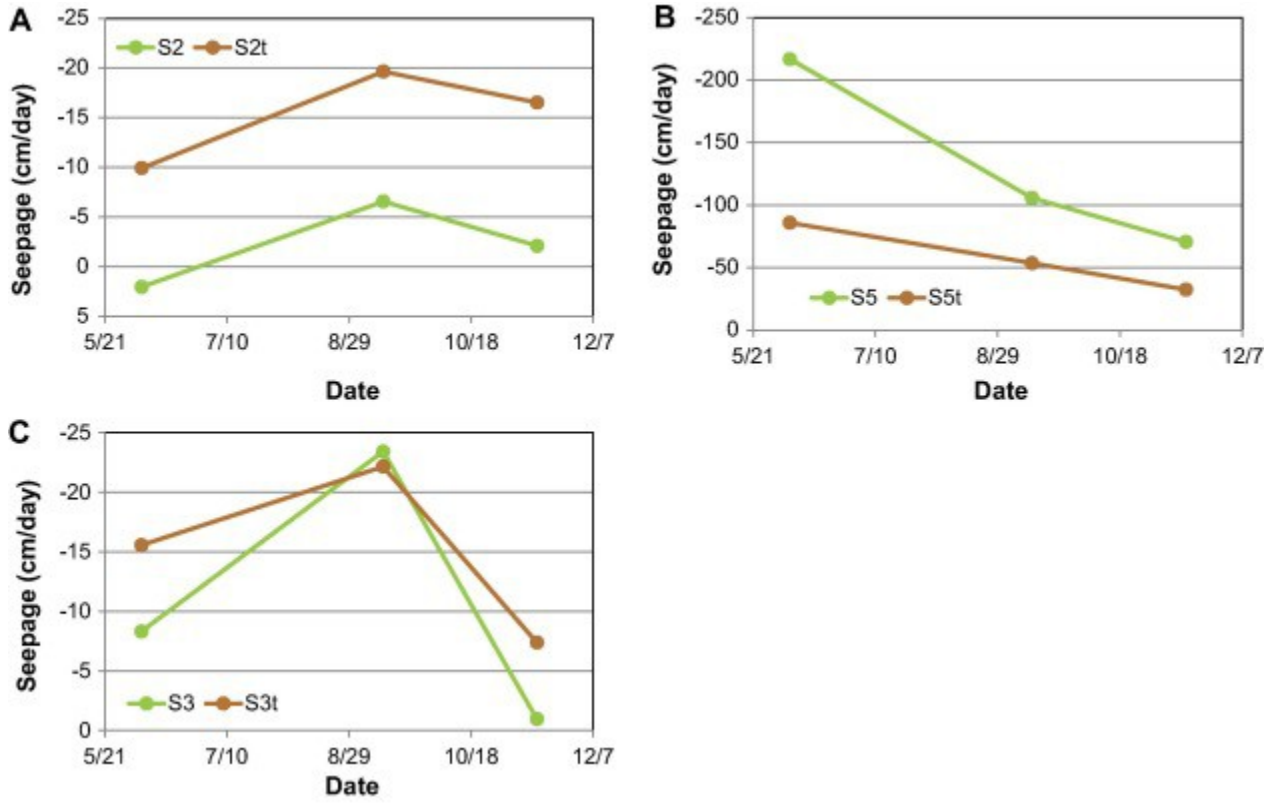

Download high-res image (276KB)
Download full-size image

Fig. 7. Comparison of seepage estimated from seepage meter (green line) and thermal probes (orange line) at (A) S2, (B) S5, and (C) S3. (For interpretation of the references to color in this figure legend, the reader is referred to the web version of this article.)

4.4. ERT results

ERT data were collected along two profiles and during four campaigns to monitor changes in subsurface saturation over time. In Fig. 1A the collector well laterals project into the imaging plane at ~90 m along the profile B–B′. Fig. 8 shows the inversion results for the May, July, September, and November data sets. Less than 5% difference in electrical resistivity after temperature correction was observed when comparing the May (base line data set) data versus the monitoring data sets (July, September and November). Based on typical laboratory resistivity values for saturated sands and gravels (~245 Ω m; Reynolds, 2011), the ERT profiles suggest that the subsurface sediments appear to be saturated during May, soon after the riverbed was inundated following dam inflation. Subsequent time-lapse images from July through November show resistivity values that increase from right to left (East to West bank). Resistivity values generally become more resistive throughout the season. July resistivity values (Fig. 8) show a dramatic increase in the amplitude and connectedness of this higher resistivity zone (>245 Ω m). September inversion results reveal a resistivity decrease around 50 m but an increase at 15 m. The November ERT results show a continued increase in amplitude and horizontal extent of the resistive feature, which extends across most of the river and is roughly 5 m thick. From July through November the top of the resistive feature is consistently 1.5–2 m below the riverbed. Annotated above each time lapse inversion image is the location of the point measurements and corresponding seepage values at those time intervals and the thalweg location.

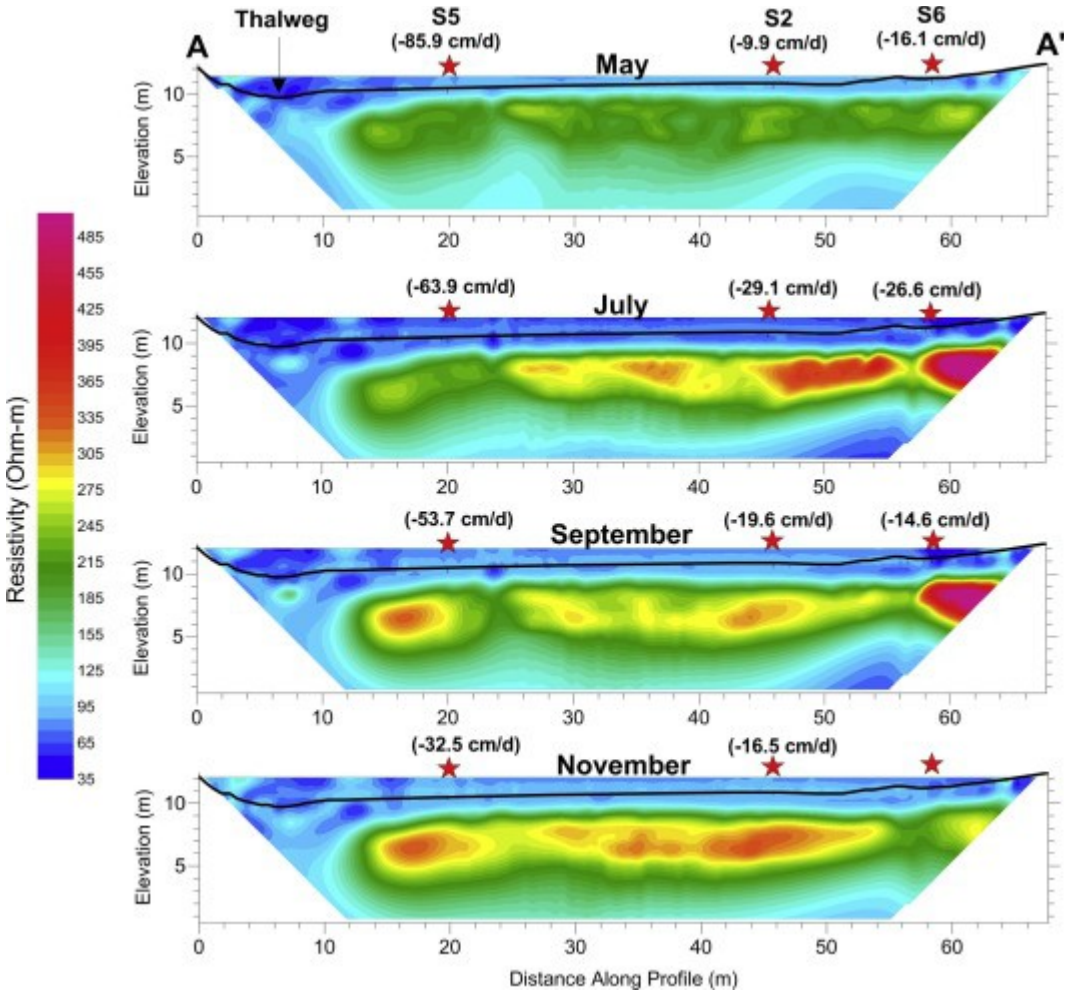

1. Download high-res image (532KB)
2. Download full-size image

Fig. 8. ERT inversion results for A–A′. ERT from May, July, September, and November. The seepage meter locations and corresponding seepage rates during that data collection period are annotated above the plots. The black line near the top of the ERT profile is the riverbed surface.

The model inversions for the ERT profile along the center axis of the river (B–B′) are shown in Fig. 9 from May to November. Again, the resistivity values of the subsurface sediments during May are very uniform except for around 40 m, where a small secondary channel bisects the ERT profile. The July data indicate a dramatic increase in resistivity from 8 m to 5 m elevation and a resistivity increase from the riverbed surface down to 8 m elevation, suggesting that the shallow surface sediments became more saturated after being exposed prior to inundation. The resistivity of the shallow sediments remains constant throughout the rest of the season. Interestingly, overall resistivity values decrease in September from July and then become more resistive again in November.

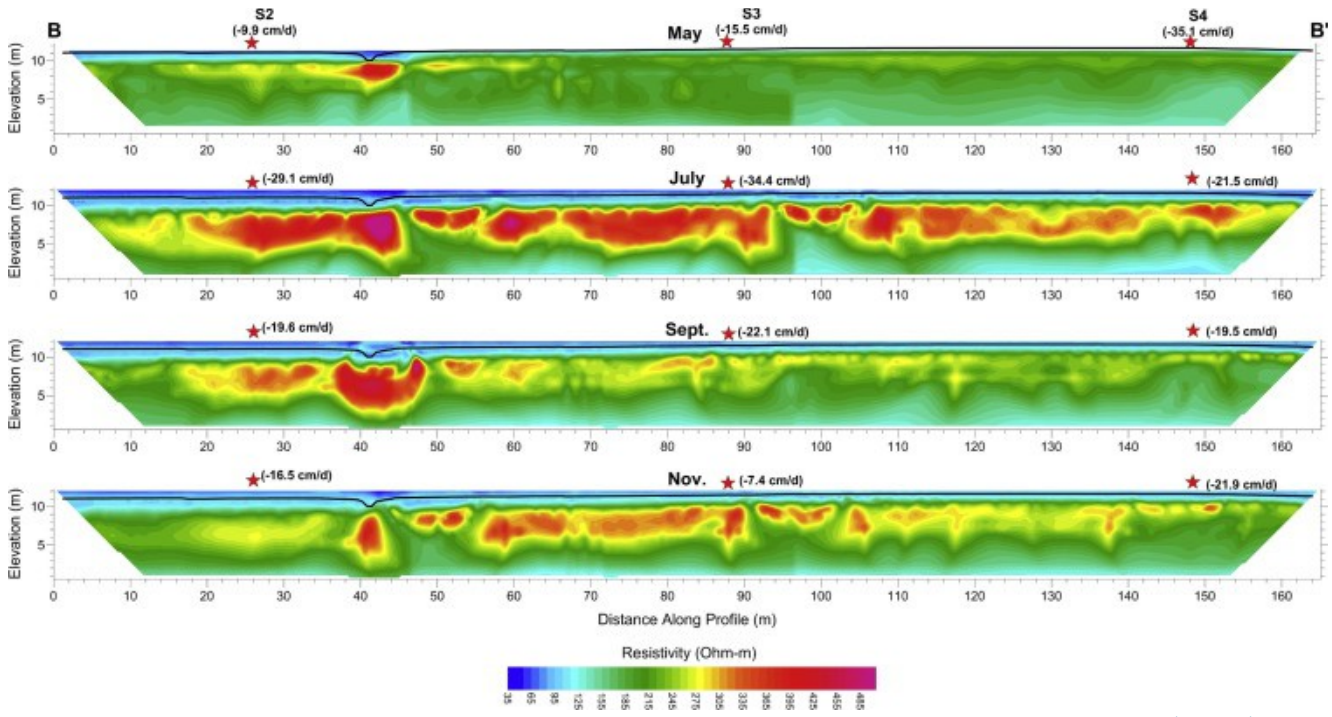

Download high-res image (663KB)
Download full-size image

Fig. 9. ERT results for B–B′ from May, July, September, and November. The seepage meter locations and corresponding seepage rates during that data collection period are annotated above the plots. The black line near the top of the ERT profile is the riverbed surface.

5. Discussion

5.1. Clogging mechanism

One of the key study objectives is to determine whether clogging at the Wohler RBF was abiotic or biotic in nature, or both, where biotic processes refer to biomass development in the riverbed. Grain-size analysis (Fig. 3A and B) did not show a consistent increase in fine-grained sediment throughout the season. Analysis of the percent change of all fine-grained sediment indicates only an average increase of approximately 2% throughout the season. This is substantially less than the amount that has been reported to be necessary to decrease seepage (e.g. Nowinski et al., 2011). Microbial analysis of colocated cores showed a substantial increase in biomass; approximately one order of magnitude increase from May to September and nearly another order of magnitude increase from September to November. Fig. 5C and D show that biomass continually increased throughout the season at all locations and to depths of 10 cm. Hydraulic conductivity estimated from grain-size analysis is spatially and temporally variable (Fig. 4). The estimated hydraulic conductivity trends are similar to seepage-meter trends, which suggest that the late season decrease in seepage (Fig. 6, Fig. 7) is likely not governed by sediment deposition, but by continued late season increases in biomass.

5.2. Influence of clogging on infiltration

To further investigate the clogging mechanisms influencing infiltration, analysis of riverbed seepage versus river stage, pumping rate (10 mgd), river velocity and surface-water temperature was performed. Fig.

10 displays seepage rate at S2 and S3 plotted against river stage. River stage increased gradually from May 29 to July 18. During this time, Fig. 10 shows seepage increased, which is the expected response due to the increase in head gradient beneath the riverbed. River stage remains constant after July 20th while seepage remains constant until approximately August 24th, seepage then starts a slow decrease throughout the rest of the season even though river stage remains constant. This behavior suggests the late season seepage decrease was due to clogging.

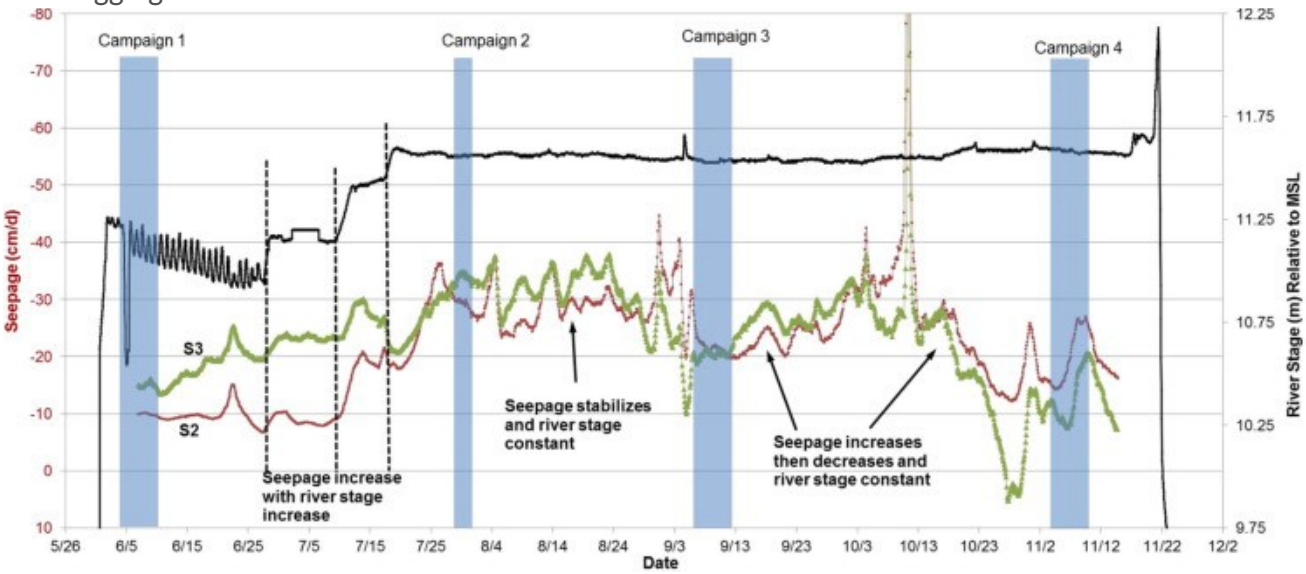

Download high-res image (194KB)
Download full-size image

Fig. 10. Seepage at S2 (red) and S3 (green) obtained from temperature sensors at 0.25 m depth versus seasonal river stage. Data collection campaigns are indicated by blue bars. (For interpretation of the references to color in this figure legend, the reader is referred to the web version of this article.)

The relationship between seepage and cumulative pumping rates associated with Collector wells 1 and 2 was also explored (Supplementary Fig. S2). The results suggest that seepage is much more affected by season than by pumping rate, or that the interpretation of late-season biological clogging governs overall system behavior. These results agree with the Zhang et al. (2011)findings, which indicate infiltration is more sensitive to riverbed permeability than to river stage or pumping rate.

Fig. 11 illustrates the same thermal seepage responses as in Fig. 10and S2 (in Supplemental Information) but illustrates the influence of seasonal temperatures and river velocity on seasonal seepage. River temperatures begin to decrease at the beginning of August throughout the remainder of the season. Seepage remains constant through much of August and begins to decrease in early September indicating that other factors control seasonal seepage rates. No stream gage was present at the site, river discharge was obtained from USGS gage located about 15 km upstream from the study area (Russian River near Healdsburg, CA, USGS station number 11465390, http://waterdata.usgs.gov/nwis) and velocities were calculated using the cross-section (A–A′) of the river at our site. River velocity decreases after the dam is raised and stabilizes around 10 cm/s until the end of October when the wet season begins and flow starts to increase. On September 3rd a large transient river pulse raises the river velocity to over 20 cm/s. According to the Hjulstrom diagram (Hjulström, 1935), which describes the mobility of different size sediments at different velocities, sediments below 1 mm will start to remobilize (erosion) and become suspended at velocities over 20 cm/s. This suggests

that the transient river pulse on 9/3/12, only days before the September campaign, could have redistributed the fine clogging layer resulting in increased seepage on subsequent days. After October 1st, the river velocity starts to gradually increase throughout the remainder of October and November, while seepage continues to decrease as river velocities near 20 cm/s (Fig. 11). Fig. 11indicates that the clogging layer continues to develop (decreasing seepage) after the September transient river pulse even as the river velocities gradually increase.

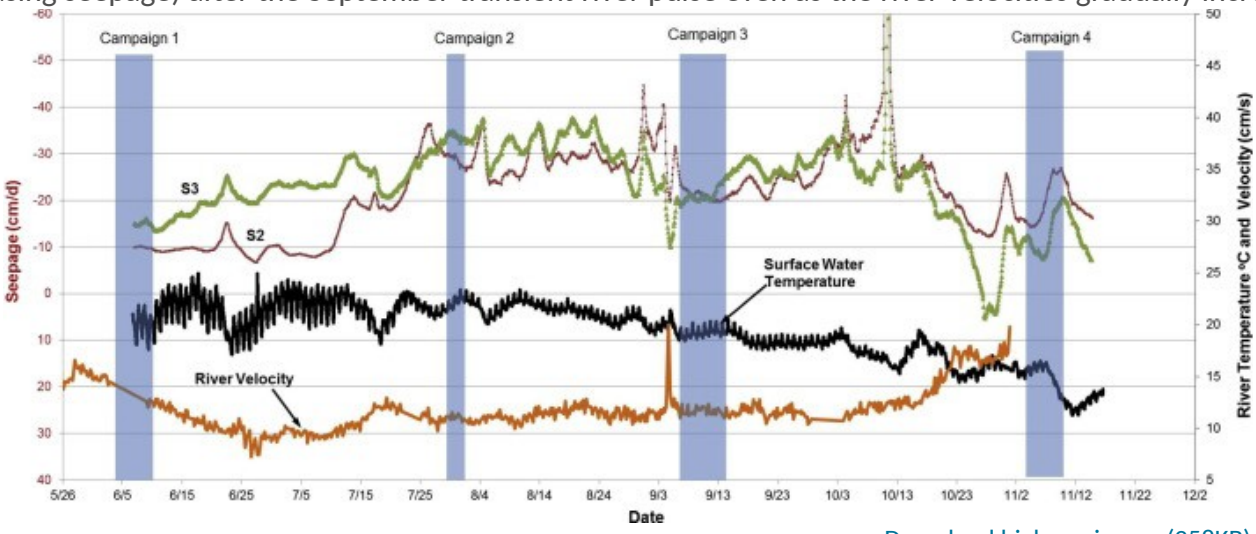

Download high-res image (258KB)
Download full-size image

Fig. 11. Thermal seepage at S2 and S3 versus river temperature and river velocity throughout the season. Data collection campaigns are indicated by blue bars. (For interpretation of the references to color in this figure legend, the reader is referred to the web version of this article.)

Su et al., 2007, Zhang et al., 2011 predicted the development of an unsaturated zone 2 m beneath the riverbed as a result of a reduction in riverbed permeability and increased pumping rate. If we apply temperature corrections to resistivity data (Eq. (2), Supplemental Information), and assume negligible changes in fluid chemistry and lithology throughout the season, it is reasonable to interpret that the increases in resistivity are due to drying and that the decreases in resistivity are due to wetting. The ERT results in Fig. 8, Fig. 9 show an increase in resistivity (above 245-Ω m) at approximately 2–5 m below the riverbed surface. Three drive-point piezometers were installed 10-m before the S5 location at 1-, 1.25-, and 1.5-m depths to confirm the presence of the unsaturated zone. The 1.5-m piezometer went dry while the collector wells were pumping; the others remained saturated. This suggests that the ERT data are likely imaging the top of the pumping-induced unsaturated zone, and gives us confidence in interpreting the spatial extent of the zone. Spatial interpolation of the pumping-induced unsaturated zone based on the ERT data (not shown) suggests that the zone can occupy an area of ∼2065 m^2 or a volume of ∼10,325 m^3. This modest interpolation is based on the vertical and lateral size of the unsaturated zone observed in the ERT profiles and the estimated zone of pumping influence for this study site, described by Su et al., 2007, Zhang et al., 2011.

5.3. Monitoring method comparison

The final objective of the study was to determine the optimal method or combination of methods for monitoring riverbed dynamic permeability. Multiple methods were tested, including point-based methods (coring, piezometers) and methods that integrated over larger footprints (ERT) and time intervals (seepage

meters, and temperature sensors). Based on our analysis and comparison of individual datasets, we found that three methods in particular provided a wealth of information about the RBF system.

- Cryocoring permitted direct collection of relatively undisturbed sediment and is reasonably inexpensive. There are some environmental health and safety hazards associated with the use of liquid nitrogen that might pose limitations for use.

- Temperature logging provided dense temporal information about seepage. Temperature-based seepage rates were mostly greater than seepage-meter values at 2 of three sites, but were substantially smaller than seepage-meter values at the site on the thalweg shoulder where seepage was fastest (Fig. 6, Fig. 7). However, the much greater frequency of temperature-based measurements provided a much improved understanding of spatiotemporal dynamics. Multiple vertical data loggers allow estimation of seepage rates at different depths below the riverbed, which seepage meters could not. The accuracy, cost, size, battery life (1 yr+), capability of holding thousands of measurements, and autonomous capability make this method invaluable for monitoring RBF operations.

- ERT permitted monitoring of the spatial extent of the pumping-induced unsaturated zone that would be difficult to do using point measurements. ERT and sediment grain-size analyses can be used collectively to interpret clogging effects on infiltration. ERT systems are relatively inexpensive, field portable, sensitive to numerous hydrological properties, and relatively easy to process, and ERT offers a way to get extensive spatial coverage to better understand sub-stream architecture and processes. Unlike cryo-cores and manual seepage meters, this method can be deployed once and set to collect autonomously, providing high temporal resolution.

6. Conclusions

This study documented that riverbed permeability at the Wohler RBF facility is spatially and temporally variable. The first ~1.25 months following the dam inflation marked a period of increasing seepage, due to the increased hydraulic gradient. Seepage then reached a steady state until about September, at which time permeability decreased. We interpret the decrease to be due primarily to the formation and accumulation of biomass. We also evaluated the effects of river stage, pumping operations, and river temperature and velocity and found small scale, short duration effects on the seasonal changes in riverbed seepage. We also observed the unsaturated zone persisted for several months and varied in space and time. Ongoing statistical and modeling research is assessing the relative influence of these different factors on infiltration at the Wohler Site (Newcomer et al., 2013).

Our experience suggested that joint use of cryocoring, temperature loggers, and ERT provides a useful measurement suite for monitoring riverbed clogging and seepage processes. Cryocoring overcame limitations associated with conventional mechanical sampling approaches to provide representative grain-size and biomass information which allowed determination of the clogging mechanism. Temperature based seepage gave seepage information consistent with seepage meters but was easier to collect and provided autonomous

and thus temporally dense information. ERT provided spatially extensive and non-invasive information about the spatial distribution of the pumping induced unsaturated zone that was consistent with point measurements.

Research is ongoing to better quantify the clogging mechanism over seasonal timescales in order to understand the complex interplay and transitions between biotic and abiotic riverbed clogging during seasonal changes and engineering operations. This study has documented an approach for such studies and has assessed the value of information provided by different monitoring methods.

Acknowledgements

The authors would like to thank Jay Jasperse and George Lincoln (Sonoma County Water Agency) for their data and insights, and Gabriella Vozza (UC Berkeley) for her help in the rock lab sieving cores and installing instrumentation during the May campaign. We would also like to thank Baptiste Dafflon and Boris Faybishenko for insights and suggestions during the formulation of this project and publication, and John Callaway for insights and use of his cryocorer. We acknowledge the funding support by Sonoma County Water Agency. Use of brand names is for informational purposes only and does not constitute endorsement by the authors, Lawrence Berkeley National Laboratory, U.S. Geological Survey, University of California, Santa Barbara, and Sonoma County Water Agency.

References

1. Archie, 1942 G.E. Archie **The electrical resistivity log as an aid in determining some reservoir characteristics**
   Transactions of the AIME, 146 (1942), pp. 54-62
2. Battin and Sengschmitt, 1999 T. Battin, D. Sengschmitt **Linking sediment biofilms, hydrodynamics, and river bed clogging: evidence from a large river**
   Microb. Ecol., 37 (3) (1999), pp. 185-196
3. Baveye et al., 1998 P. Baveye, P. Vandevivere, B.L. Hoyle, P.C. DeLeo, D.S. de Lozada **Environmental impact and mechanisms of the biological clogging of saturated soils and aquifer materials**
   Crit. Rev. Environ. Sci. Technol., 28 (2) (1998), pp. 123-191
4. Bianchin et al., 2011 M. Bianchin, L. Smith, R. Beckie **Defining the hyporheic zone in a large tidally influenced river**
   J. Hydrol., 406 (1) (2011), pp. 16-29
5. Binley and Kemna, 2005 A. Binley, A. Kemna **DC resistivity and induced polarization methods**
   Hydrogeophysics, Springer (2005), pp. 129-156
6. Blasch et al., 2007 Blasch, K.W., Constantz, J., Stonestrom, D.A., 2007. Thermal Methods for Investigating Ground-water Recharge, US Geological Survey Professional Paper 1703, appendix 1.
7. Blaschke et al., 2003 A.P. Blaschke, K.H. Steiner, R. Schmalfuss, D. Gutknecht, D.Sengschmitt **Clogging processes in hyporheic interstices of an impounded river, the Danube at Vienna, Austria**
   Int. Rev. Hydrobiol., 88 (3–4) (2003), pp. 397-413
8. Bouskill et al., 2012 N.J. Bouskill, H.C. Lim, S. Borglin, R. Salve, T.E. Wood, W.L.Silver, E.L. Brodie **Pre-exposure to drought increases the resistance of tropical forest soil bacterial communities to extended drought**
   ISME J., 7 (2) (2012), pp. 384-394

9. Bunte and Abt, 2001 Bunte, K., Abt, S.R., 2001. Sampling Surface and Subsurface Particle-size Distributions in Wadable Gravel-and Cobble-bed Streams for Analyses in Sediment Transport, Hydraulics, and Streambed Monitoring, US Department of Agriculture, Forest Service, Rocky Mountain Research Station Fort Collins, Colorado.
10. Cahoon et al., 1996 D.R. Cahoon, J.C. Lynch, R.M. Knaus **Improved cryogenic coring device for sampling wetland soils: research method paper**
J. Sediment. Res., 66 (5) (1996)
11. Cardenas and Markowski, 2010 M.B. Cardenas, M.S. Markowski **Geoelectrical imaging of hyporheic exchange and mixing of river water and groundwater in a large regulated river**
Environ. Sci. Technol., 45 (4) (2010), pp. 1407-1411
12. Chapuis, 2012 R. Chapuis **Predicting the saturated hydraulic conductivity of soils: a review**
Bull. Eng. Geol. Environ., 71 (3) (2012), pp. 401-434
13. Constable et al., 1987 S.C. Constable, R.L. Parker, C.G. Constable **Occam's inversion: a practical algorithm for generating smooth models from electromagnetic sounding data**
Geophysics, 52 (3) (1987), pp. 289-300
14. Constantz, 2008 J. Constantz **Heat as a tracer to determine streambed water exchanges**
Water Resour. Res., 44 (4) (2008)
15. Constantz et al., 2004 Constantz, J., Su, G., Hatch, C., 2004. Heat as a Tracer to Examine Hydraulic Conductance Near the Russian River Bank Filtration Facility, Report Number LBNL-58021, Lawrence Berkeley National Laboratory, Sonoma County, CA.
16. Cox et al., 2007 M.H. Cox, G.W. Su, J. Constantz **Heat, chloride, and specific conductance as ground water tracers near streams**
Ground Water, 45 (2) (2007), pp. 187-195
17. Crook et al., 2008 N. Crook, A. Binley, R. Knight, D. Robinson, J. Zarnetske, R.Haggerty **Electrical Resistivity Imaging of the Architecture of Substream Sediments**
Water Resour. Res., 44 (2008), p. W00D13, 10.1029/2008WR006968
18. Cunningham et al., 1987 A. Cunningham, C. Anderson, H. Bouwer **Effects of sediment-laden flow on channel bed clogging**
J. Irrigation Drain. Eng., 113 (1) (1987), pp. 106-118
19. Cusack et al., 2010 D.F. Cusack, W.L. Silver, M.S. Torn, S.D. Burton, M.K.Firestone **Changes in microbial community characteristics and soil organic matter with nitrogen additions in two tropical forests**
Ecology, 92 (3) (2010), pp. 621-632
20. Darnault et al., 2003 C.J. Darnault, P. Garnier, Y.-J. Kim, K.L. Oveson, T.S.Steenhuis, J.-Y. Parlange, M. Jenkins, W.C. Ghiorse, P. Baveye **Preferential transport of *Cryptosporidium parvum* oocysts in variably saturated subsurface environments**
Water Environ. Res. (2003), pp. 113-120
21. Dean, 1974 W.E. Dean **Determination of carbonate and organic matter in calcareous sediments and sedimentary rocks by loss on ignition; comparison with other methods**
J. Sediment. Res., 44 (1) (1974), pp. 242-248
22. deGroot-Hedlin and Constable, 1990 C. deGroot-Hedlin, S. Constable **Occam's inversion to generate smooth, two-dimensional models from magnetotelluric data**
Geophysics, 55 (12) (1990), pp. 1613-1624
23. Engesgaard et al., 2006 Engesgaard, P., Seifert, D., Herrera, P., 2006. Bioclogging in porous media: tracer studies. In: Riverbank Filtration Hydrology, pp. 93–118.
24. Flemming et al., 2007 H.-C. Flemming, M. Strathmann, C.F.L. Morales **Microbial effects**

B. Westrich, U. Forstner (Eds.), Sediment Dynamics and Pollutant Mobility in Rivers-An Interdisciplinary Approach, Springer-Verlag (2007), pp. 343-378

25. Gordon et al., 2012 R.P. Gordon, L.K. Lautz, M.A. Briggs, J.M. McKenzie **Automated calculation of vertical pore-water flux from field temperature time series using the VFLUX method and computer program**
J. Hydrol., 420 (2012), pp. 142-158
26. Gorman, 2004 Gorman, P.D., 2004. Spatial and Temporal Variability of Hydraulic Properties in the Russian River Streambed, Central Sonoma County, California [Masters: San Francisco State University].
27. Griffiths et al., 1998 B. Griffiths, K. Ritz, N. Ebblewhite, G. Dobson **Soil microbial community structure: effects of substrate loading rates**
Soil Biol. Biochem., 31 (1) (1998), pp. 145-153
28. Guckert et al., 1985 J.B. Guckert, C.P. Antworth, P.D. Nichols, D.C. White **Phospholipid, ester-linked fatty acid profiles as reproducible assays for changes in prokaryotic community structure of estuarine sediments**
FEMS Microbiol. Lett., 31 (3) (1985), pp. 147-158
29. Günther et al., 2006 T. Günther, C. Rücker, K. Spitzer **Three-dimensional modelling and inversion of dc resistivity data incorporating topography—II**
Inversion Geophys. J. Int., 166 (2) (2006), pp. 506-517
30. Hanrahan et al., 2005 T.P. Hanrahan, D.R. Geist, E.V. Arntzen **Habitat quality of historic Snake River fall Chinook salmon spawning locations and implications for incubation survival. Part 1: Substrate quality**
River Res. Appl., 21 (5) (2005), pp. 455-467
31. Hatch, 2007 Hatch, C.E., 2007. Spatial and Temporal Dynamics of Surface Water–groundwater Interactions Using Time-series Analysis of Streambed Thermal Records in Coastal Streams, University of California, Santa Cruz.
32. Hatch et al., 2006 C.E. Hatch, A.T. Fisher, J.S. Revenaugh, J. Constantz, C. Ruehl **Quantifying surface water–groundwater interactions using time series analysis of streambed thermal records: method development**
Water Resour. Res., 42 (10) (2006)
33. Hazen, 1892 Hazen, A., 1892. Some physical properties of sands and gravels: with special reference to their use in filtration. In: Massachusetts State Board of Health, 24th Annual Report. Publication No. 34, pp. 539–556.
34. Heiri et al., 2001 O. Heiri, A.F. Lotter, G. Lemcke **Loss on ignition as a method for estimating organic and carbonate content in sediments: reproducibility and comparability of results**
J. Paleolimnol., 25 (1) (2001), pp. 101-110
35. Hjulström, 1935 F. Hjulström **Studies of the Morphological Activity of Rivers as Illustrated by the River Fyris: Inaugural Dissertation**
Almqvist & Wiksells (1935)
36. Hoffmann and Gunkel, 2011 A. Hoffmann, G. Gunkel **Bank filtration in the sandy littoral zone of Lake Tegel (Berlin): structure and dynamics of the biological active filter zone and clogging processes**
Limnologica Ecol. Manage. Inland Waters, 41 (1) (2011), pp. 10-19
37. Hubbs, 2004 Hubbs, S.A., Processes involved in mechanical clogging of riverbank filtration systems. In: Proceedings NATO Advanced Research Workshop on Riverbank Filtration: Effect of Riverbed Clogging on Water Quality and System Capacity, 2004, Samorin-Cilistov Bratislava, Slovak Republic.
38. Hubbs, 2006 Hubbs, S.A., 2006. Evaluating streambed forces impacting the capacity of riverbed filtration systems. In: Riverbank Filtration Hydrology, pp. 21–42.
39. Jaramillo, 2012 M. Jaramillo **Riverbank filtration: an efficient and economical drinking-water treatment technology**
Dyna, 79 (171) (2012), pp. 148-157
40. Keller and Frischknecht, 1996 G.V. Keller, F.C. Frischknecht **Electrical Methods in Geophysical Prospecting**

Pergamon Press (1996)

41. Kondolf et al., 2005 G.M. Kondolf, T.E. Lisle, G.M. Wolman **Bed Sediment Measurement Tools in Fluvial Geomorphology**
John Wiley & Sons, Ltd. (2005) p. 347–395
42. Kozeny, 1927 J. Kozeny **Ueber kapillare leitung des wassers im boden: Sitzungsber**
Akad. Wiss. Wien, 136 (1927), pp. 271-306
43. Lautz, 2012 L.K. Lautz **Observing temporal patterns of vertical flux through streambed sediments using time-series analysis of temperature records**
J. Hydrol., 464 (2012), pp. 199-215
44. Lee and Cherry, 1979 D.R. Lee, J.A. Cherry **A field exercise on groundwater flow using seepage meters and mini-piezometers**
J. Geol. Educ., 27 (1) (1979), pp. 6-10
45. Lesmes and Friedman, 2005 D. Lesmes, S. Friedman **Relationships between the electrical and hydrogeological properties of rocks and soils**
Y. Rubin, S. Hubbard (Eds.), Hydrogeophysics, vol. 50, Springer, Netherlands (2005), pp. 87-128
46. Lisle, 1989 T.E. Lisle **Sediment transport and resulting deposition in spawning gravels, north coastal California**
Water Resour. Res., 25 (6) (1989), pp. 1303-1319
47. Miller et al., 2008 C.R. Miller, P.S. Routh, T.R. Brosten, J.P. McNamara **Application of time-lapse ERT imaging to watershed characterization**
Geophysics, 73 (3) (2008), pp. G7-G17
48. Mitchell et al., 2008 Mitchell, N., Nyquist, J.E., Toran, L., Rosenberry, D., Mikochik, J., Electrical resistivity as a tool for identifying geologic heterogeneities which control seepage at Mirror Lake. In: Proceedings Symposium on the Application of Geophysics to Engineering and Environmental Problems (SAGEEP), 2008, pp. 749–759.
49. Moore-Kucera and Dick, 2008 J. Moore-Kucera, R.P. Dick **PLFA profiling of microbial community structure and seasonal shifts in soils of a Douglas-fir chronosequence**
Microb. Ecol., 55 (3) (2008), pp. 500-511
50. Moser et al., 2003 D.P. Moser, J.K. Fredrickson, D.R. Geist, E.V. Arntzen, A.D.Peacock, S.M.W. Li, T. Spadoni, J.P. McKinley **Biogeochemical processes and microbial characteristics across groundwater-surface water boundaries of the Hanford Reach of the Columbia River**
Environ. Sci. Technol., 37 (22) (2003), pp. 5127-5134
51. Naranjo et al., 2012 R.C. Naranjo, R.G. Niswonger, M. Stone, C. Davis, A. Mckay **The use of multiobjective calibration and regional sensitivity analysis in simulating hyporheic exchange**
Water Resour. Res., 48 (1) (2012)
52. Newcomer et al., 2013 Newcomer, M.E., Hubbard, S.S., Fleckenstein, J.H., Schmidt, C., Maier, U., Thullner, M., Rubin, Y., Dynamic Permeability and Clogging Processes of Riverbank Filtration Systems. In: Proceedings AGU, San Francisco, CA, 2013.
53. Nogaro et al., 2010 G. Nogaro, T. Datry, F. Mermillod-Blondin, S. Descloux, B.Montuelle **Influence of streambed sediment clogging on microbial processes in the hyporheic zone**
Freshw. Biol., 55 (6) (2010), pp. 1288-1302
54. Nowinski et al., 2011 J.D. Nowinski, M.B. Cardenas, A.F. Lightbody **Evolution of hydraulic conductivity in the floodplain of a meandering river due to hyporheic transport of fine materials**
Geophys. Res. Lett., 38 (1) (2011), p. L01401
55. Nyquist et al., 2008 J.E. Nyquist, P.A. Freyer, L. Toran **Stream bottom resistivity tomography to map ground water discharge**
Ground Water, 46 (4) (2008), pp. 561-569

56. Nyquist et al., 2009 J.E. Nyquist, M.J. Heaney, L. Toran **Characterizing lakebed seepage and geologic heterogeneity using resistivity imaging and temperature measurements**
    Near Surf. Geophys. (2009), 10.3997/1873-0604.2009022
57. Nyquist et al., 2010 Nyquist, J.E., Toran, L., Fang, A.C., Ryan, R.J., Rosenberry, D., Tracking tracer breakthrough in the hyporheic zone using time-lapse DC resistivity, Crabby Creek, Pennsylvania. In: 23rd EEGS Symposium on the Application of Geophysics to Engineering and Environmental Problems, 2010.
58. Odong, 2007 J. Odong **Evaluation of empirical formulae for determination of hydraulic conductivity based on grain-size analysis**
    J. Am. Sci., 3 (3) (2007), pp. 54-60
59. Pfiffner et al., 2006 S.M. Pfiffner, J.M. Cantu, A. Smithgall, A.D. Peacock, D.C.White, D.P. Moser, T.C. Onstott, E. van Heerden **Deep subsurface microbial biomass and community structure in Witwatersrand Basin mines**
    Geomicrobiol J., 23 (6) (2006), pp. 431-442
60. Ray and Prommer, 2006 C. Ray, H. Prommer**Clogging-induced flow and chemical transport simulation in riverbank filtration systems**
    S.A. Hubbs (Ed.), Riverbank Filtration Hydrology, Springer, Netherlands(2006), pp. 155-177
61. Reynolds, 2011 J.M. Reynolds **An Introduction to Applied and Environmental Geophysics**
    John Wiley & Sons (2011)
62. Revil and Glover, 1998 A. Revil, P. Glover **Nature of surface electrical conductivity in natural sands, sandstones, and clays**
    Geophys. Res. Lett., 25 (5) (1998), pp. 691-694
63. Revil and Glover, 1997 A. Revil, P.W.J. Glover **Theory of ionic-surface electrical conduction in porous media**
    Phys. Rev. B, 55 (3) (1997), pp. 1757-1773
64. Rosenberry, 2005 D.O. Rosenberry **Integrating seepage heterogeneity with the use of ganged seepage meters**
    Limnol. Oceanography Meth., 3 (2005), pp. 131-142
65. Rosenberry, 2008 D.O. Rosenberry **A seepage meter designed for use in flowing water**
    J. Hydrol., 359 (1–2) (2008), pp. 118-130
66. Rosenberry et al., 2012 D.O. Rosenberry, P.Z. Klos, A. Neal **In situ quantification of spatial and temporal variability of hyporheic exchange in static and mobile gravel-bed rivers**
    Hydrol. Process., 26 (4) (2012), pp. 604-612
67. Rosenberry and Pitlick, 2009 D.O. Rosenberry, J. Pitlick **Local-scale variability of seepage and hydraulic conductivity in a shallow gravel-bed river**
    Hydrol. Process., 23 (23) (2009), pp. 3306-3318
68. Salant, 2011 N.L. Salant **'Sticky business': the influence of streambed periphyton on particle deposition and infiltration**
    Geomorphology, 126 (3) (2011), pp. 350-363
69. Salomonová et al., 2003 S. Salomonová, J. Lamačová, M. Rulík, J. Rolčíkc, L.Čápa, P. Bednáře, P. Barták **Determination of phospholipid fatty acids in sediments**
    Facultas Rerum Naturalium, 42 (2003), pp. 39-49
70. Schälchli, 1992 U. Schälchli **The clogging of coarse gravel river beds by fine sediment**
    Hydrobiologia, 235 (1) (1992), pp. 189-197
71. Schijven et al., 2003 J. Schijven, P. Berger, I. Miettinen **Removal of pathogens, surrogates, indicators, and toxins using Riverbank Filtration**
    C. Ray, G. Melin, R.B. Linksy (Eds.), Riverbank Filtration: Improving Source Water-Quality, Kluwer Academic Publishers, Dordrecht, The Netherlands (2003), pp. 73-116
72. Schubert, 2006a J. Schubert **Experience with riverbed clogging along the Rhine River**

S.A. Hubbs (Ed.), Riverbank Filtration Hydrology, Springer, Netherlands (2006), pp. 221-242

73. Schubert, 2006b J. Schubert **Significance of hydrologic aspects on RBF performance**
S.A. Hubbs (Ed.), Riverbank Filtration Hydrology, vol. 60, Springer, Netherlands (2006), pp. 1-20
74. Schwartz et al., 2008 B.F. Schwartz, M.E. Schreiber, T. Yan **Quantifying field-scale soil moisture using electrical resistivity imaging**
J. Hydrol., 362 (3–4) (2008), pp. 234-246
75. Seifert and Engesgaard, 2007 D. Seifert, P. Engesgaard **Use of tracer tests to investigate changes in flow and transport properties due to bioclogging of porous media**
J. Contam. Hydrol., 93 (1) (2007), pp. 58-71
76. Shanafield et al., 2011 M. Shanafield, C. Hatch, G. Pohll **Uncertainty in thermal time series analysis estimates of streambed water flux**
Water Resour. Res., 47 (3) (2011)
77. Singha and Gorelick, 2006 K. Singha, S.M. Gorelick **Effects of spatially variable resolution on field-scale estimates of tracer concentration from electrical inversions using Archie's law**
Geophysics, 71 (3) (2006), pp. G83-G91
78. Slater et al., 2010 L.D. Slater, D. Ntarlagiannis, F.D. Day-Lewis, K.Mwakanyamale, R.J. Versteeg, A. Ward, C. Strickland, C.D. Johnson, J.W.Lane Jr. **Use of electrical imaging and distributed temperature sensing methods to characterize surface water–groundwater exchange regulating uranium transport at the Hanford 300 Area, Washington**
Water Resour. Res., 46 (10) (2010), p. W10533
79. Sophocleous, 2002 M. Sophocleous **Interactions between groundwater and surface water: the state of the science**
Hydrogeol. J., 10 (1) (2002), pp. 52-67
80. Steger et al., 2003 K. Steger, Å. Jarvis, S. Smårs, I. Sundh **Comparison of signature lipid methods to determine microbial community structure in compost**
J. Microbiol. Methods, 55 (2) (2003), pp. 371-382
81. Stuyfzand et al., 2006 P.J. Stuyfzand, M.H.A. Juhàsz-Holterman, W.J. Lange **Riverbank filtration in the Netherlands: Well fields, clogging and geochemical reactions**
S.A. Hubbs (Ed.), Riverbank Filtration Hydrology, Springer, Netherlands (2006), pp. 119-153
82. Su et al., 2003 G.W. Su, J. James, D. Seymour, J. Constantz **Analysis of temperatures and water levels in wells to estimate alluvial aquifer hydraulic conductivities**
Ground Water, 42 (2003)
83. Su et al., 2004 G.W. Su, J. Jasperse, D. Seymour, J. Constantz **Estimation of hydraulic conductivity in an alluvial system using temperatures**
Ground Water, 42 (6) (2004), pp. 890-901
84. Su et al., 2007 G.W. Su, J. Jasperse, D. Seymour, J. Constantz, Q. Zhou **Analysis of pumping-induced unsaturated regions beneath a perennial river**
Water Resour. Res., 43 (8) (2007)
85. Thullner et al., 2002 M. Thullner, J. Zeyer, W. Kinzelbach **Influence of microbial growth on hydraulic properties of pore networks**
Transp. Porous Media, 49 (1) (2002), pp. 99-122
86. Toran et al., 2013 L. Toran, J.E. Nyquist, A.C. Fang, R.J. Ryan, D.O. Rosenberry **Observing lingering hyporheic storage using electrical resistivity: variations around stream restoration structures, Crabby Creek, PA**
Hydrol. Proc., 27 (10) (2013), pp. 1411-1425

87. Treese et al., 2009 S. Treese, T. Meixner, J.F. Hogan **Clogging of an effluent dominated semiarid river: a conceptual model of stream-aquifer interactions(1)**
J. Am. Water Resour. Assoc., 45 (4) (2009), pp. 1047-1062
88. Tufenkji et al., 2002 N. Tufenkji, J.N. Ryan, M. Elimelech **Peer reviewed: the promise of bank filtration**
Environ. Sci. Technol., 36 (21) (2002), pp. 422-428
89. Vandevivere and Baveye, 1992 P. Vandevivere, P. Baveye **Saturated hydraulic conductivity reduction caused by aerobic bacteria in sand columns**
Soil Sci. Soc. Am. J., 56 (1) (1992), pp. 1-13
90. Vukovic and Soro, 1992 M. Vukovic, A. Soro **Determination of Hydraulic Conductivity of Porous Media from Grain-size Distribution**
Water Resources Publications, LLC (1992)
91. Ward et al., 2012 A.S. Ward, M. Fitzgerald, M.N. Gooseff, T.J. Voltz, A.M. Binley, K. Singha **Hydrologic and geomorphic controls on hyporheic exchange during base flow recession in a headwater mountain stream**
Water Resour. Res., 48 (4) (2012), p. W04513
92. Ward et al., 2010 A.S. Ward, M.N. Gooseff, K. Singha **Imaging hyporheic zone solute transport using electrical resistivity**
Hydrol. Process., 24 (7) (2010), pp. 948-953
93. Wett, 2006 B. Wett **Monitoring clogging of a RBF-system at the river Enns, Austria**
S.A. Hubbs (Ed.), Riverbank Filtration Hydrology (2006), pp. 259-280
94. White and Ringelberg, 1998 D.C. White, D.B. Ringelberg **Signature Lipid Biomarker Analysis**
Oxford University Press, New York (1998)
95. Young et al., 2010 P.C. Young, C.J. Taylor, W. Tych, D. Pedregal, P.G. McKenna **The Captain toolbox, Centre for Research on Environmental Systems and Statistics**
Lancaster University (2010)
96. Zhang et al., 2011 Y.Q. Zhang, S. Hubbard, S. Finsterle **Factors governing sustainable groundwater pumping near a river**
Ground Water, 49 (3) (2011), pp. 432-444
97. Zimmermann et al., 2005 A. Zimmermann, M. Coulombe-Pontbriand, M. Lapointe**Biases of submerged bulk and freeze-core samples**
Earth Surf. Proc. Land., 30 (11) (2005), pp. 1405-1417